Finite-Element Analysis of Three-Dimensional Axisymmetrical Invisibility Cloaks and Other Metamaterial Devices

Yong Bo Zhai, Xue Wei Ping, Wei Xiang Jiang and Tie Jun Cui*

State Key Laboratory of Millimeter Waves and the Institute of Target Characteristics and Identification, Department of Radio Engineering, Southeast University, Nanjing 210096, China.

Abstract. Accurate simulations of metamaterial devices are very important in the analysis of their electromagnetic properties. However, it is very difficult to make full-wave simulations of three-dimensional (3D) metamaterial devices due to the huge memory requirements and long computing time. In this paper, we present an efficient finite-element method (FEM) to analyze 3D axisymmetric electromagnetic devices designed by the transformation-optics approach, such as invisibility cloaks and concentrators. In the proposed method, we use the edge-based vector basis functions to expand the transverse field components, and the node-based scalar basis functions to expand the angular component. The FEM mesh is truncated with a cylindrical perfectly matched layer. We have applied the method to investigate the scattering from spherical and ellipsoidal invisibility cloaks and circularly cylindrical concentrators, in which the permittivity and permeability are both inhomogeneous and anisotropic. Numerical results are presented to show the validity and efficiency of the method.

AMS subject classifications: 52B10, 65D18, 68U05, 68U07

Key words: Finite-element method, axisymmetrical scatterer, metamaterial devices.

1 Introduction

Recently, invisibility cloaks based on metamaterials have aroused great interest [1–5]. Pendry et al. first proposed a coordinate transformation approach to provide a new method to control electromagnetic (EM) fields, by which a space consisting of the free

*Corresponding author. *Email addresses:* ybzhai@emfield.org (Y. B. Zhai), xwping@emfield.org (X. W. Ping), wxjiang@emfield.org (W. X. Jiang), tjcui@seu.edu.cn (T. J. Cui)

space can be squeezed into a new space with different volume and space-distributed constitutive parameters [1]. Following this approach, a two-dimensional (2D) microwave invisibility cloak was experimentally realized [2], and some other metamaterial devices, such as the EM-wave concentrators [6,7], rotators [8], and hyperlens [9,10] have also been investigated by similar methods.

Besides experiments, the numerical simulation is the other important approach to analyze the EM properties of metamaterial devices. So far, several methods have been used to simulate the invisibility cloaks. The ray-tracing simulations [1,2] supporting the conclusions by Pendry et al. [1] were reported in the geometric optics limit. The full-wave finite-element simulations [3] were performed to study the effects of cloaking material perturbations to the propagation of the incident waves in a 2D cylindrical case. A rigorous solution to Maxwell's equations for a spherical cloak has been reported in [5]. The discrete dipole approximation method has been applied to simulate three-dimensional (3D) spherical cloaks and irregular 3D cloaks approximately [11,12]. However, the full-wave analysis and simulations of complicated 3D cloaks are still limited due to the large amount of computational burden and memory requirements. For example, the commercial software, COMSOL Multiphysics, which has been widely used in 2D situations, cannot be used to analyze large 3D cloaks and other metamaterial devices since the huge memory requirements and computational time.

The finite-element method (FEM) is characterized by the very flexible material handling capabilities and is often preferred for problems involving complex structures and inhomogeneous anisotropic materials [13,14]. By taking advantage of the rotational symmetry, the 3D problem can be reduced to a 2D computational domain. In this paper, an efficient FEM is proposed and applied to investigate the scattering from 3D axisymmetrical metamaterial devices designed by the transformation-optics approach, such as the invisibility cloaks and concentrators, whose permittivity and permeability are both inhomogeneous and anisotropic. In the proposed method, we use the edge-based vector basis functions to expand the transverse field components and the node-based scalar basis functions to expand the angular component, which automatically constrains the tangential field components to be continuous and eliminate the problem of spurious solutions without the need for a penalty factor. Triangular elements are applied to conveniently and accurately model arbitrary shapes of body of revolution. The FEM mesh is truncated with a cylindrical perfectly matched layer (PML) [13–15], which is much more efficient for arbitrarily-shaped scatterers than is a spherical boundary. The accurately numerical results are presented to show the validity and efficiency of the method.

2   FEM formulations for 3D axisymmetrical metamaterial devices

A metamaterial device with the PML enclosure is shown in Fig. 1. It is assumed here that the symmetric axis of axisymmetric metamaterial device with inhomogeneous and
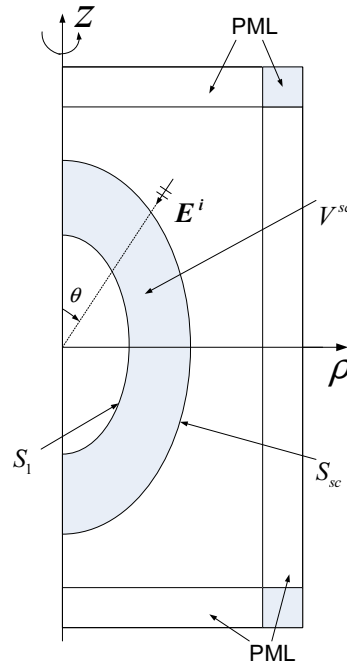
Figure 1: Slice of a metamaterial device with the PML enclosure.

anisotropic permittivity and permeability is the z-axis for a right-handed cylindrical co-ordinate system (ρ,ϕ,z). For the anisotropic metamaterial, the relative permittivity tensor $\bar{\bar{\epsilon}}_a$ and permeability tensor $\bar{\bar{\mu}}_a$ have the following symmetric forms

$$\bar{\bar{\epsilon}}_a = \frac{1}{\epsilon_0} \begin{pmatrix} \epsilon_{\rho\rho} & 0 & \epsilon_{\rho z} \\ 0 & \epsilon_{\phi\phi} & 0 \\ \epsilon_{\rho z} & 0 & \epsilon_{zz} \end{pmatrix}, \qquad \bar{\bar{\mu}}_a = \frac{1}{\mu_0} \begin{pmatrix} \mu_{\rho\rho} & 0 & \mu_{\rho z} \\ 0 & \mu_{\phi\phi} & 0 \\ \mu_{\rho z} & 0 & \mu_{zz} \end{pmatrix}. \tag{2.1}$$

The domain is truncated with a cylindrical PML, which is conveniently interpreted as an anisotropic medium with $\bar{\bar{\mu}}_p$ and $\bar{\bar{\epsilon}}_p$ a diagonal tensor. Thus the relative permeability and permittivity tensors for PML can be written as

$$\bar{\bar{\mu}}_p = \bar{\bar{\epsilon}}_p = \frac{1}{\epsilon_0} \left(\hat{\rho}\hat{\rho}\epsilon_{\rho\rho}^p + \hat{\phi}\hat{\phi}\epsilon_{\phi\phi}^p + \hat{z}\hat{z}\epsilon_{zz}^p \right),$$

and a discussion of appropriate functions for $\epsilon_{\rho\rho}^p$, $\epsilon_{\phi\phi}^p$, and ϵ_{zz}^p can be found in [13–15]. The PML to air interface is reflectionless in the cylindrical coordinates, and waves which propagate through the PML is attenuated. Hence any convenient boundary condition can be applied on the outer mesh boundary. In the following derivation and simulations, the medium parameters of the core anisotropic metamaterial, the intermediate air region, and the outer PML can be generally expressed by $\bar{\bar{\epsilon}}_r$ and $\bar{\bar{\mu}}_r$, as shown in Fig. 1. The tensors $\bar{\bar{\mu}}_r$ and $\bar{\bar{\epsilon}}_r$ also contain the information of isotropic medium, for which $\epsilon_{\rho\rho} = \epsilon_{\phi\phi} = \epsilon_{zz} = \epsilon_0\epsilon_r$, $\mu_{\rho\rho} = \mu_{\phi\phi} = \mu_{zz} = \mu_0\mu_r$, and $\epsilon_{\rho z} = \mu_{\rho z} = 0$.

From the Maxwell's equations, the vector wave equation for the inhomogeneous and anisotropic medium can be derived as

$$\nabla \times (\bar{\bar{\mu}}_r^{-1} \cdot \nabla \times \mathbf{E}) - k_0^2 \bar{\bar{\epsilon}}_r \cdot \mathbf{E} = 0, \tag{2.2}$$

where $k_0 = \omega \sqrt{\mu_0 \epsilon_0}$ is the free space wavenumber. If the metamaterial device contains a perfectly electric conductor (PEC), for example, an invisible cloak, the PEC boundary conditions are used with

$$\hat{n} \times \mathbf{E} = 0, \quad \text{on } S_1, \tag{2.3}$$

where S_1 is the PEC surface, as shown in Fig. 1. According to the generalized variational principle [16], the functional for this problem is given by the following equation

$$F(\mathbf{E}) = \frac{1}{2} \iiint_V \left[(\nabla \times \mathbf{E}) \cdot \bar{\bar{\mu}}_r^{-1} \cdot (\nabla \times \mathbf{E}) - k_0^2 \mathbf{E} \cdot \bar{\bar{\epsilon}}_r \cdot \mathbf{E} \right] dV. \tag{2.4}$$

For the scattering problem, it is more efficient to calculate the scattering field than the total field. Thus, $\mathbf{E} = \mathbf{E}^\mathbf{i} + \mathbf{E}^\mathbf{s}$ is substituted into Eq. (2.4), and terms that do not depend on $\mathbf{E}^\mathbf{s}$ are dropped. This yields

$$\begin{aligned}
F(\mathbf{E}^\mathbf{s}) = &\frac{1}{2} \iiint_V \left[(\nabla \times \mathbf{E}^\mathbf{s}) \cdot \bar{\bar{\mu}}_r^{-1} \cdot (\nabla \times \mathbf{E}^\mathbf{s}) - k_0^2 \mathbf{E}^\mathbf{s} \cdot \bar{\bar{\epsilon}}_r \cdot \mathbf{E}^\mathbf{s} \right] dV \\
&+ \iint_{V^{sc}} \left[(\nabla \times \mathbf{E}^\mathbf{s}) \cdot \bar{\bar{\mu}}_r^{-1} \cdot (\nabla \times \mathbf{E}^\mathbf{i}) - k_0^2 \mathbf{E}^\mathbf{s} \cdot \bar{\bar{\epsilon}}_r \cdot \mathbf{E}^\mathbf{i} \right] dV \\
&- \iint_{S_{sc}} \mathbf{E}^\mathbf{s} \cdot (\hat{n} \times \nabla \times \mathbf{E}^\mathbf{i}) dS, \tag{2.5}
\end{aligned}$$

in which S_{sc} is the surface of penetrable scatterer V^{sc} (the metamaterial device), and $\hat{n}$ on S_{sc} points from the free space region into the scatterer region.

To take advantage of the rotational symmetry of the problem, the fields are expanded in the Fourier modes as [13,17]

$$\mathbf{E} = \sum_{m=-\infty}^{+\infty} \left[\mathbf{E}_{t,m}(\rho,z) + \hat{\phi} \mathbf{E}_{\phi,m}(\rho,z) \right] e^{jm\phi}, \tag{2.6}$$

where

$$\mathbf{E}_{\phi,0}^s = \sum_{i=1}^{3} e_{\phi,i}^e N_i^e, \qquad \mathbf{E}_{t,0}^s = \sum_{i=1}^{3} e_{t,i}^e \mathbf{N}_i^e, \qquad \text{for} \quad m=0, \tag{2.7a}$$

$$\mathbf{E}_{\phi,\pm1}^s = \sum_{i=1}^{3} e_{\phi,i}^e N_i^e, \qquad \mathbf{E}_{t,\pm1}^s = \sum_{i=1}^{3} \left[\mp j \hat{\rho} e_{\phi,i}^e N_i^e + e_{t,i}^e \rho \mathbf{N}_i^e \right], \qquad \text{for} \quad m=\pm1, \tag{2.7b}$$

$$\mathbf{E}_{\phi,m}^s = \sum_{i=1}^{3} e_{\phi,i}^e N_i^e, \qquad \mathbf{E}_{t,m}^s = \sum_{i=1}^{3} e_{t,i}^e \rho \mathbf{N}_i^e, \qquad \text{for} \quad |m|>1. \tag{2.7c}$$

in which N_i^e is a standard 2D nodal-element basis function, and $\mathbf{N}_i^e$ is a standard 2D edge-element basis function. The expansions in Eq. (2.6) are substituted into Eq. (2.4) and the functional is differentiated with respect to the unknown coefficients and then the result is set to zero. This process yields a sparse, symmetric matrix equation

$$\begin{pmatrix} A_{tt}^m & A_{t\phi}^m \\ A_{\phi t}^m & A_{\phi\phi}^m \end{pmatrix} \begin{pmatrix} e_t^m \\ e_\phi^m \end{pmatrix} = \begin{pmatrix} B_t^m \\ B_\phi^m \end{pmatrix}, \tag{2.8}$$

where $m = 0, \pm 1, \pm 2, \cdots$.

　　The FEM matrix for a given mode number m is stored compactly and the matrix equation can be solved according the techniques described in [18]. The above procedure should in principle be carried out for each of the Fourier modes, where $m = 0, \pm 1, \pm 2, \cdots$. In practice, however, a rule of truncating the infinite Fourier modes is $M_{\max} = k_0 \rho_{\max} \sin\theta + 6$ [19], where ρ_{max} is the largest cylindrical radius of the scatterer. This rule is valid for $k_0 \rho_{\max} \sin\theta > 3$. Furthermore, as shown in [13], the solution for each negative modes ($m < 0$) is simply related to that of the corresponding positive modes ($m > 0$). Hence the solutions need to be computed for the nonnegative modes only ($m = 0, 1, 2, \cdots$).

3　Full-wave simulations of 3D axisymmetrical invisibility cloaks and concentrators

A number of numerical results are presented to show the validity and capability of the proposed FEM technique for 3D axisymmetrical metamaterial devices. Because of the strong inhomogeneity and anisotropy of the scatterer, the mesh length for each example is about $\lambda_d/20$, where λ_d is the equivalent wavelength in medium. After the assembly and solution of the finite element system matrix to obtain the degrees of freedom for every mode m, the scattered electric field for arbitrary position (ρ, ϕ, z) near the scatterer is calculated by Eq. (2.6). The total field can be obtained by adding the incident electric field to the scattered electric field, which can be transformed into Cartesian coordinate by Eq. (3.1):

$$\begin{pmatrix} E_x \\ E_y \\ E_z \end{pmatrix} = \begin{pmatrix} \cos\phi & -\sin\phi & 0 \\ \sin\phi & \cos\phi & 0 \\ 0 & 0 & 1 \end{pmatrix} \begin{pmatrix} E_\rho \\ E_\phi \\ E_z \end{pmatrix}. \tag{3.1}$$

For the following examples, the total field in the two orthogonal cuts on the x-z plane and x-y plane is illustrated and information about the resources to compute the results is given in Table 1. The commercial software COMSOL Multiphysics can be used to analyze 3D cloaks and other metamaterial devices using 3D finite element method. However, it is very inefficient since the huge memory requirements and computational time. For example, about seventy thousands unknowns, 5GB memory and 3 hours are needed to simulate the $8/3\lambda$ cylindrical concentrator.

Table 1: Computational statistics to compute near field.

Target	Number of unknowns	Memory (MB)	CPU time (s)
6λ spherical cloak	148,261	570	44
6λ spherical cloak with thickness 0.6λ	197,765	711	39
10λ spherical cloak	394,848	1,700	182
8λ rotating spheroidal cloak	197,129	748	72
16λ rotating spheroidal cloak	404,059	1,200	107
$8/3\lambda$ cylindrical concentrator, parallel incidence/oblique incidence	92,588	350	14/171

First, we consider a spherical cloak with free space inside so that we compare the simulation results with Mie-series analytical results [5] to validate the accuracy of the proposed FEM technique. Fig. 2 shows the resulting simulated real part of electric field in the vicinity of the spherical cloak with the permittivity and permeability tensors described by [1]

$$\bar{\bar{\mu}}_a = \bar{\bar{\epsilon}}_a = \hat{r}\hat{r}\epsilon_r + \hat{\theta}\hat{\theta}\epsilon_\theta + \hat{\phi}\hat{\phi}\epsilon_\theta, \tag{3.2}$$

where

$$\epsilon_r = \frac{R_2}{R_2 - R_1} \frac{(r - R_1)^2}{r^2}, \qquad \epsilon_\theta = \frac{R_2}{R_2 - R_1},$$

and R_1 and R_2 are the inner and outer radii of the spherical cloak, respectively. The above equations can be transformed into the cylindrical coordinate as

$$\bar{\bar{\mu}}_a = \bar{\bar{\epsilon}}_a = \begin{pmatrix} \epsilon_r \sin^2\theta + \epsilon_\theta \cos^2\theta & 0 & (\epsilon_r - \epsilon_\theta)\sin\theta\cos\theta \\ 0 & \epsilon_\theta & 0 \\ (\epsilon_r - \epsilon_\theta)\sin\theta\cos\theta & 0 & \epsilon_\theta \sin^2\theta + \epsilon_r \cos^2\theta \end{pmatrix}, \tag{3.3}$$

where we choose $R_2 = 2R_1 = 3\lambda$, and the cloaked region is free space.

Fig. 2 illustrates the real parts of E_x in the two orthogonal cuts on the x-z plane and x-y plane. From the figure, we clearly observe that the cloaking effect is very clear and the plane wave is almost unaltered outside the cloaking shell, which is nearly the same as the analytical result [5]. Also, the electric field inside the cloaked region is nearly zero, in which a maximum leakage about 3.3% of the radiating field into the cloaked region is observed due to the discretization error of material properties.

Fig. 3 demonstrates the simulation result of an electrically large cloaked PEC sphere, whose diameter is 4.8λ with a cloaked layer of thickness 0.6λ. Clearly, the result remains accurate for the electrically larger object with thinner cloaking shell. From Figs. 2 and 3, we also find that the fields outside the cloaking shells are not sensitive to the medium inside the cloaked region. Fig. 4 shows the electric-field distribution for a bigger cloak with $R_2 = 2R_1 = 5\lambda$. There is a maximum leakage of 12% of the radiating field into the cloaked region, which is lager than that in Fig. 2.
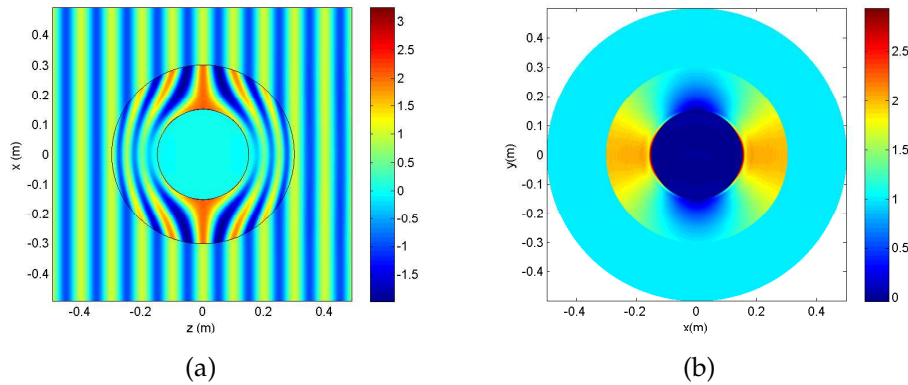
(a)   (b)

Figure 2: The real part of the electric field E_x in the vicinity of the cloaked sphere with $R_2 = 2R_1 = 3\lambda$. The incident plane wave propagates from the left to the right. (a) The electric-field in x-z plane. (b) The electric-field in x-y plane.
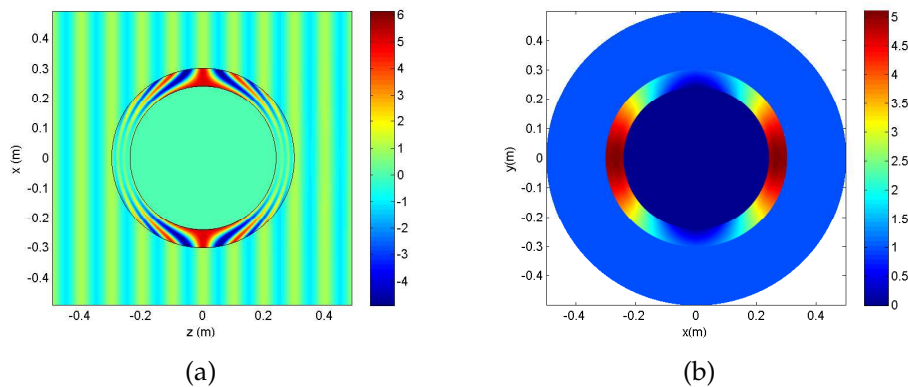

(a)   (b)

Figure 3: The electric field distribution in the vicinity of the larger cloaked PEC sphere with thinner cloaking shell. (a) The electric-field in x-z plane. (b) The electric-field in x-y plane.

(a)   (b)
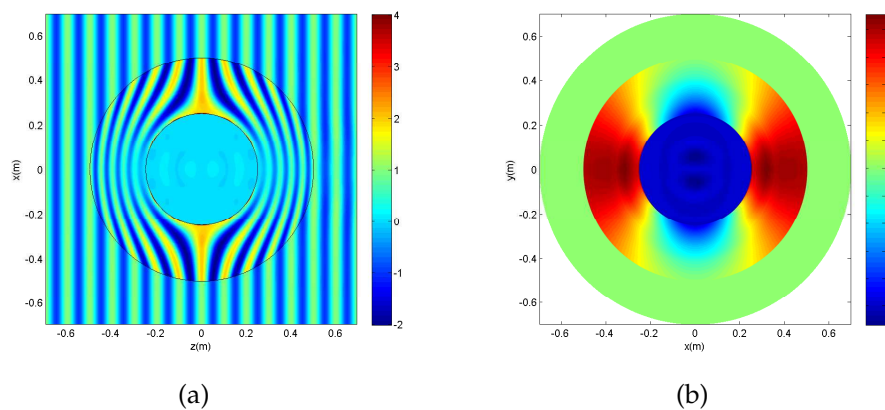
Figure 4: The electric field distribution of the spheroidal with $R_2 = 2R_1 = 5\lambda$. The incident plane wave propagates from the left to the right. (a) The electric-field in x-z plane. (b) The electric-field in x-y plane.
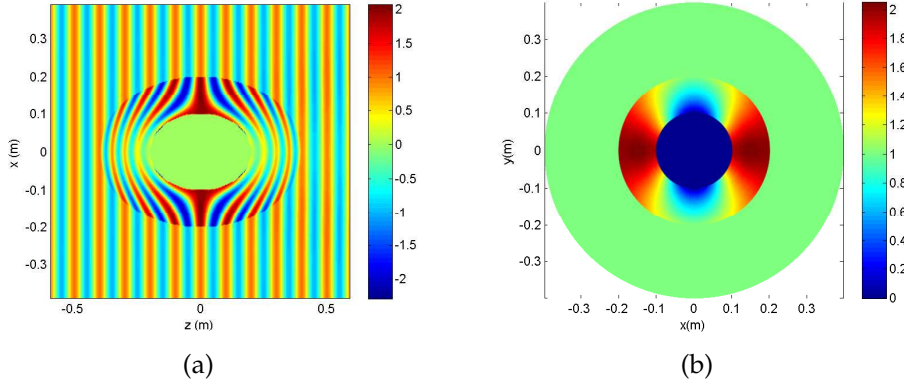
Figure 5: The electric field distribution of the spheroidal cloak with $b=2a=2\lambda$, and $k=2$. (a) The electric-field in x-z plane. (b) The electric-field in x-y plane.
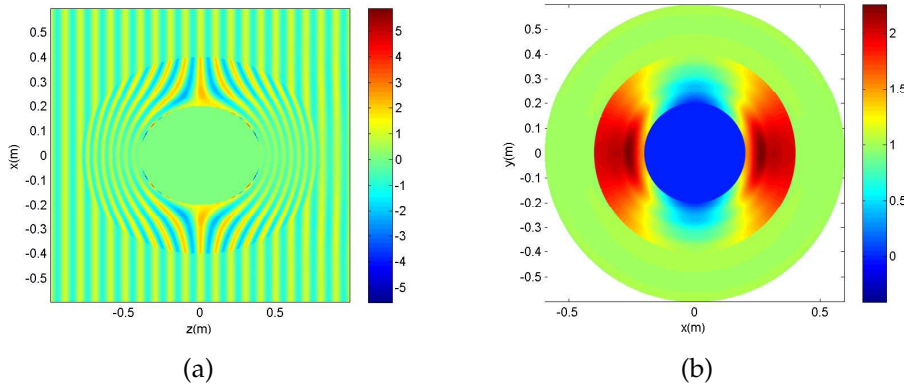

Figure 6: The electric field distribution of the spheroidal cloak with $b=2a=4\lambda$, and $k=2$. (a) The electric-field in x-z plane. (b) The electric-field in x-y plane.

Next we consider a rotating spheroidal cloak, which is an extension of 2D elliptical cloaks [20, 21]. Assume that the semi-axes of the inner and outer ellipsoid are a and b in the x and y directions, and the semi-axes are ka and kb in the z direction. Based on the transformation equation given in [22], the permittivity and permeability tensors are derived in the cylindrical coordinates as

$$\bar{\bar{\mu}}_a=\bar{\bar{\epsilon}}_a=\frac{b}{(b-a)t^6}\begin{pmatrix} (t^3-\kappa_1)^2+\kappa_2^2 & 0 & -(t^3-\kappa_1)\kappa_3-\kappa_2(t^3-\kappa_4) \\ 0 & t^6 & 0 \\ -(t^3-\kappa_1)\kappa_3-\kappa_2(t^3-\kappa_4) & 0 & (t^3-\kappa_4)^2+\kappa_3^2 \end{pmatrix}, \quad (3.4)$$

where $t=\sqrt{k^2\rho^2+z^2}$, $\kappa_1=k^3a\rho^2$, $\kappa_2=ka\rho z$, $\kappa_3=k^3a\rho z$, $\kappa_4=kaz^2$, and $\rho=\sqrt{x^2+y^2}$. In our simulations, we set $b=2a=2\lambda$, and $k=2$. The cloaked region is free space. Fig. 5 illustrates the electric field distributions of the rotating spheroidal cloak. Clearly, the plane waves outside the cloak keep their original propagation directions. The maximum

leakage of the radiating field into the cloaked region is slightly larger than that of the spherical cloak because of the stronger inhomogeneity and anisotropy of the spheroidal cloak. Fig. 6 demonstrates the results of larger spheroidal cloak when $b=2a=4\lambda$ and the cloaked region is PEC, from which we see that the cloaking effect is also very clear.
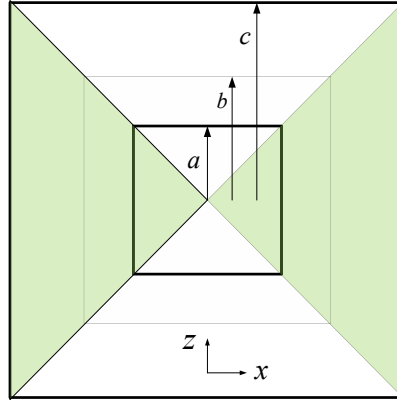

Figure 7: A circularly cylindrical concentrator with inner diameter and height equal to $2a$ and outer diameter and height equal to $2c$.

Finally, to show the application of the method to other kinds of metamaterial devices designed by the transformation optics, we consider a circularly cylindrical concentrator illuminated by the plane waves. It is impossible to get the analytical results by solving Maxwell's equations due to the very irregular structure of the scatterer. The cylindrical concentrator can be considered as an extension of 2D square concentrator [23]. The transformation equation for the cylindrical concentrator with inner diameter and height equal to $2a$ and outer diameter and height equal to $2c$ (see Fig. 7) are expressed as

$$x' = \begin{cases} ax/b, & 0 \leq \rho \leq b, \\ (k_1 - k_2 c / \sqrt{x^2+y^2})x, & b < \rho \leq c, \end{cases} \tag{3.5}$$

$$y' = \begin{cases} ay/b, & 0 \leq \rho \leq b, \\ (k_1 - k_2 c / \sqrt{x^2+y^2})y, & b < \rho \leq c, \end{cases} \tag{3.6}$$

$$z' = \begin{cases} az/b, & 0 \leq \rho \leq b, \\ (k_1 - k_2 c / \sqrt{x^2+y^2})z, & b < \rho \leq c, \end{cases} \tag{3.7}$$

for $|z| < \rho$ and $0 \leq \phi \leq 2\pi$, in which $k_1 = (c-a)/(c-b)$, $k_2 = (b-a)/(c-b)$, and $\rho = \sqrt{x^2+y^2}$. Here, (x,y,z) are the Cartesian coordinates of the original space, while (x',y',z') are the Cartesian coordinates of the transformed space. The corresponding transformation formulas for the upper and lower domain of the cylindrical concentrator are then given by

$$x' = \begin{cases} ax/b, & 0 \leq |z| \leq b, \\ (k_1 - k_2 c / |z|)x, & b < |z| \leq c, \end{cases} \tag{3.8}$$

$$y' = \begin{cases} ay/b, & 0 \le |z| \le b, \\ (k_1 - k_2 c/|z|)y, & b < |z| \le c, \end{cases} \tag{3.9}$$

$$z' = \begin{cases} az/b, & 0 \le |z| \le b, \\ (k_1 - k_2 c/|z|)z, & b < |z| \le c. \end{cases} \tag{3.10}$$

From the above transformation equations, the space is compressed into a cylindrical region with radius a at the expense of an expansion of the space between a and c. Then the permittivity and permeability tensors are derived. We have eliminated any dependence on the components of (x,y,z) in the original space, hence we can now drop the primes for aesthetic reasons. For $a < \rho \le c$, $-c \le z \le c$, $|z| < \rho$ and $0 \le \phi \le 2\pi$, the permittivity and permeability tensors are expressed as

$$\bar{\bar{\mu}}_a = \bar{\bar{\epsilon}}_a = \begin{pmatrix} k_1 t^2 & 0 & k_2 czt/\rho^2 \\ 0 & \frac{1}{k_1} & 0 \\ k_2 czt/\rho^2 & 0 & \frac{1}{k_1}\left(1 + (k_2 cz/\rho^2)^2\right) \end{pmatrix}, \tag{3.11}$$

where $t = 1/k_1 + k_2 c/k_1 \rho$. The permittivity and permeability tensors for upper and lower truncated cone are shown as

$$\bar{\bar{\mu}}_a = \bar{\bar{\epsilon}}_a = \begin{pmatrix} \frac{1}{k_1}\left(1 + (k_2 c\rho/z^2)^2\right) & 0 & \pm k_2 c\rho t/z^2 \\ 0 & \frac{1}{k_1} & 0 \\ \pm k_2 c\rho t/z^2 & 0 & k_1 t^2 \end{pmatrix}, \tag{3.12}$$

where $t = 1/k_1 \pm k_2 c/k_1 z$, and the sign "$+$" is for the upper truncated cone, and "$-$" for the lower truncated cone. The permittivity and permeability for the inner cylinder are $\mu_r = \epsilon_r = b/a$.

Figs. 8 and 9 illustrate the electric field distributions of the cylindrical concentrator when the incident elevation angle is $0°$ and $45°$, respectively. 10 modes are needed for $45°$ incident elevation angle. It is obvious that the field intensities are strongly enhanced in the inner cylindrical region within the concentrator material. The simulated intensity enhancement factor for the chosen structure with $b = 3a = \lambda$ and $c = 4/3\lambda$ is 3.0, which is very consistent with the expected ratio b/a.

4   Conclusions

An efficient FEM approach was presented and applied to investigate 3D axisymmetric metamaterial devices with inhomogeneous and anisotropic permittivity and permeability. Such problems cannot be solved by the conventional commercial software due to the huge amount of memory requirements and computing time. As examples, the spherical and ellipsoidal invisibility cloaks, and cylindrical concentrators have been analyzed. The method can also be used to analyze other devices such as rotators, hyperlens, etc.
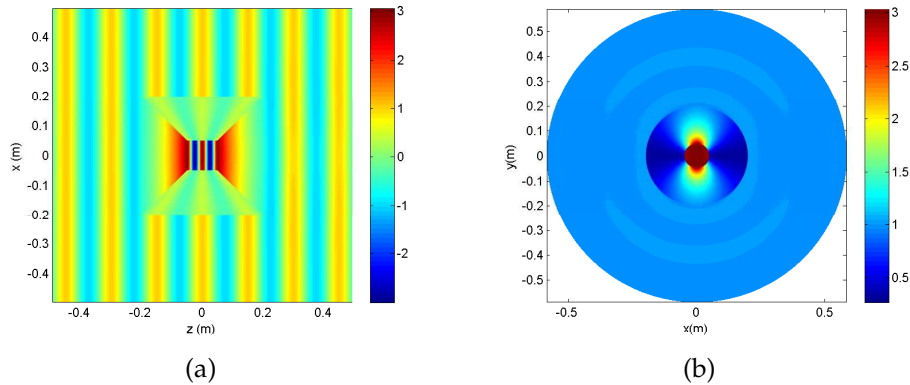
Figure 8: The electric field distribution of the cylindrical concentrator when the incident elevation angle of plane wave is $0°$. (a) The electric-field in x-z plane. (b) The electric-field in x-y plane.
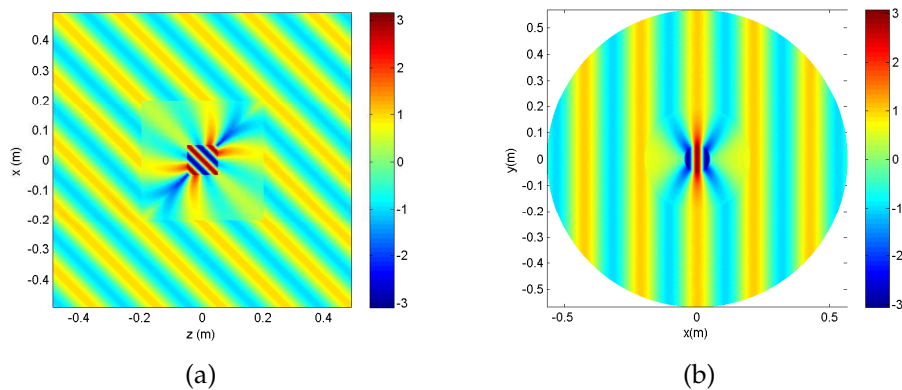

Figure 9: The electric field distribution of the cylindrical concentrator when the incident elevation angle of plane wave is $45°$. (a) The electric-field in x-z plane. (b) The electric-field in x-y plane.

Acknowledgments

References

[1] J. B. Pendry, D. Schurig and D. R. Smith, Controlling electromagnetic fields, Science., 312 (2006), 1780–1782.
[2] D. Schurig, J. B. Pendry and D. R. Smith, Calculation of material properties and ray tracing in transformation media, Opt. Express., 14 (2006), 9794–9804.

[3] S. A. Cummer, B.-I. Popa, D. Schurig, D. R. Smith and J. B. Pendry, Full-wave simulations of electromagnetic cloaking structures, Phys. Rev. E., 74 (2006), 036621.

[4] D. Schurig, J. J. Mock, B. J. Justice, S. A. Cummer, J. B. Pendry, A. F. Starr and D. R. Smith, Metamaterial electromagnetic cloak at microwave frequencies, Science., 314 (2006), 977–980.

[5] H. Chen, B.-I. Wu, B. Zhang and J. A Kong, Electromagnetic wave interactions with a metamaterial cloak, Phys. Rev. Lett., 99 (2007), 063903.

[6] M. Rahm, D. Schurig, D. A. Roberts, S. A. Cummer, D. R. Smith and J. B. Pendry, Design of electromagnetic cloaks and concentrators using form-invariant coordinate transformations of Maxwell's equations, Photo. Nanos. Fund. Appl., 6 (2008), 87–95.

[7] A. D. Yaghjian and S. Maci, Alternative derivation of electromagnetic cloaks and concentrators, New. J. Phys., 10 (2008), 115022.

[8] H. Chen and C. T. Chan, Transformation media that rotate electromagnetic fields, Appl. Phys. Lett., 90 (2007), 241105.

[9] M. Tsang and D. Psaltis, Magnifying perfect lens and superlens design by coordinate transformation, Phys. Rev. B., 77 (2008), 035122.

[10] A. V. Kildishev and E. E. Narimanov, Impedance-matched hyperlens, Opt. Lett., 32 (2007), 3432–3434.

[11] Y. You, G. W. Kattawar, P. W. Zhai and P. Yang, Zero-backscatter cloak for aspherical particles using a generalized DDA formalism, Opt. Express., 16(2008), 2068–2079.

[12] Y. You, G. W. Kattawar, P. W. Zhai and P. Yang, Invisibility cloaks for irregular particles using coordinate transformations, Opt. Express., 16 (2008), 6134–6145.

[13] A. D. Greenwood and J. M. Jin, Finite-element analysis of complex axisymmetric radiatingstructures, IEEE. T. Antenn. Propag., 47 (1999), 1260–1266.

[14] A. D. Greenwood and J. M. Jin, Computation of the RCS of a complex BOR using FEM with coupled azimuth potentials and PML, Electromagnetics., 19 (1999), 147–170.

[15] F. L. Teixeira and W. C. Chew, Systematic derivation of anisotropic PML absorbing media in cylindrical and spherical coordinates, IEEE. Microw. Guided. W., 7 (1997), 371–373.

[16] J. M. Jin, The Finite Element Method in Electromagnetics, New York: Wiley, 1993.

[17] M. F. Wong, M. Prak and V. F. Hanna, Axisymmetric edge-based finite element formulation for bodies of revolution: application to dielectric resonators, IEEE. MTT. S. Dig., (1995), 285–288.

[18] R. S. Chen, D. X. Wang, E. K. N. Yung and J. M. Jin, Application of the multifrontal method to the vector FEM for analysis of microwave filters, Microw. Opt. Tech. Lett., 31 (2001), 465–470.

[19] M. G. Andreasen, Scattering from bodies of revolution, IEEE. T. Antenn. Propag., 13 (1965), 303–310.

[20] D. H. Kwon and D. H. Werner, Two-dimensional eccentric elliptic electromagnetic cloaks, Appl. Phys. Lett., 92 (2008), 013505.

[21] W. X. Jiang, T. J. Cui, G. X. Yu, X. Q. Lin, Q. Cheng and J. Y. Chin, Arbitrarily ellipticalcylindrical invisible cloaking, J. Phys. D: Appl. Phys., 41 (2008), 085504.

[22] Q. Cheng, W. X. Jiang and T. J. Cui, Investigations of the electromagnetic properties of threedimensional arbitrarily-shaped cloaks, Prog. Electromagn. Res., 94 (2009), 105–117.

[23] W. X. Jiang, T. J. Cui, Q. Cheng, J. Y. Chin, X. M. Yang, R. Liu and D. R. Smith, Design of arbitrarily shaped concentrators based on conformally optical transformation of nonuniform rational B-spline surfaces, Appl. Phys. Lett., 92 (2008), 264101.